The Effect of the MAPS Weather Model on GPS-Determined Ellipsoidal Heights

JOHN MARSHALL, MARK SCHENEWERK, AND RICHARD SNAY *National Geodetic Survey, NOAA, NOS/NGS6, 1315 East-West Highway, Silver Spring, MD 20910*

SETH GUTMAN *Forecast Systems Laboratory, Demonstration Division, 325 Broadway, R/R/FS3, Boulder, CO 80303-3328*

We investigated a current numerical weather model, known as MAPS (Mesoscale Analysis and Prediction System), to determine if it could precisely define the behavior of GPS signals in the troposphere, ultimately leading to improved GPS-determined ellipsoidal heights. MAPS is the research version of the Rapid Update Cycle (RUC2) generated by NOAA's Forecast Systems Laboratory. MAPS is generated on an hourly basis and provides coverage in the contiguous United States at a 40-km grid spacing. We processed numerous subsets of GPS data collected over a month-long period on 23 static baselines ranging in length from 62 to 304 km. The GPS data were processed in ½-hr, 1-hr, 2-hr, and 4-hr session lengths. The primary effort was to compare the precision of heights obtained using a commonly adopted seasonal weather model with the precision of heights obtained using the MAPS weather model. Our analysis shows that the current version of MAPS can lead to improvement in GPS height precision when session lengths are shorter than two hours. For sessions longer than two hours, comparably precise heights may be obtained using a less accurate seasonal model by introducing appropriate nuisance parameters into the height estimation process. © *2001 John Wiley & Sons, Inc.*

INTRODUCTION

The precision of Global Positioning System (GPS)-determined positions continues to improve as GPS researchers construct numerical models to account for the systematic errors that corrupt GPS observations. Nevertheless, several challenging systematic errors remain inadequately modeled.

One such systematic error is the lower atmosphere that delays or slows down GPS signals, adversely affecting the precision of all GPS-determined quantities, but especially GPS-determined ellipsoidal heights. Weather fronts may cause the GPS signal delay to vary by greater than 3 centimeters over a 1-hour period (Brunner & Welsh, 1993), potentially leading to ellipsoidal height errors exceeding 9 cm. The delay caused by the lower atmosphere is referred to as the neutral atmospheric delay (NAD) and extends from the GPS antenna to the upper troposphere/lower stratosphere (~10–16 km), where atmospheric pressure approaches zero.

The hypothesis under study is whether GPS-determined ellipsoidal height precision can be improved by incorporating a priori weather data into static baseline processing, thereby diminishing the impact of systematic errors caused by the weather. The hypothesis is tested using GPS data for 23 baselines whose lengths range from 62 to 304 km and for observing sessions whose lengths range from ½ hr to 4 hr.

We analyzed several sources of a priori weather information in this study; however, the primary source of weather information was obtained from a numerical weather model called Mesoscale Analysis and Prediction System (MAPS) maintained and developed by the Forecast Systems Laboratory (FSL) of the National Oceanic and Atmospheric Administration (NOAA) (http://maps.fsl.noaa.gov/). MAPS is the research version of the Rapid Update Cycle (RUC2) that runs operationally at the

GPS Solutions, Vol. 5, No. 1, pp. 1–14 (2001)

National Centers for Environmental Prediction (NCEP). NCEP is the starting point for nearly all weather forecasts in the United States. MAPS is intended to provide high-frequency, hourly analyses of conventional and new data sources over the contiguous United States in support of aviation and other mesoscale users (Fullerton, 1999). Input to MAPS primarily consists of four types of meteorological observations including: (1) rawinsonde (a radiosonde (weather balloon) tracked by a radio direction-finding device to determine the velocity of winds aloft), (2) observations from commercial aircraft, (3) wind observations from 35 tropospheric wind profilers located mostly in the central United States, and (4) traditional surface observations of temperature, pressure, humidity and other quantities. MAPS meteorological products are provided for a 40-km grid that covers the contiguous United States. The current latency associated with the MAPS analysis product is 21 min after each hour.

In addition to the MAPS model, we analyzed the Global Positioning System-Integrated Precipitable Water (GPS-IPW) model maintained and developed by the FSL Demonstration Division (http://www.dd.fsl.noaa.gov/gps.html). Currently, the GPS-IPW model has limited spatial coverage relative to the MAPS model because GPS-IPW is based on post-processed GPS observations from roughly 60 discrete ground stations primarily located in the central plains and along U.S. coastal areas. The latency associated with the GPS-IPW product is currently approximately 30 hr. The GPS-IPW project intends to demonstrate the feasibility and utility of using surface-based GPS observations for improved weather forecasting, climate monitoring, and satellite sensor calibration/validation.

The third and final model we analyzed is the "Seasonal" model, which yields relatively crude meteorological estimates based on an empirical fit to historical climatic data (Herring, 1995). As its name implies, the Seasonal model supplies estimates of temperature, pressure, and humidity whose variations are dominated by seasonal effects; however, negligible year-to-year variations also exist. The input for the Seasonal model consists of station latitude and ellipsoidal height as well as the desired epoch of time for the meteorological estimates. Given this input, the Seasonal model returns the temperature based on coefficients from the empirical fit, the pressure based on a crude relationship between pressure

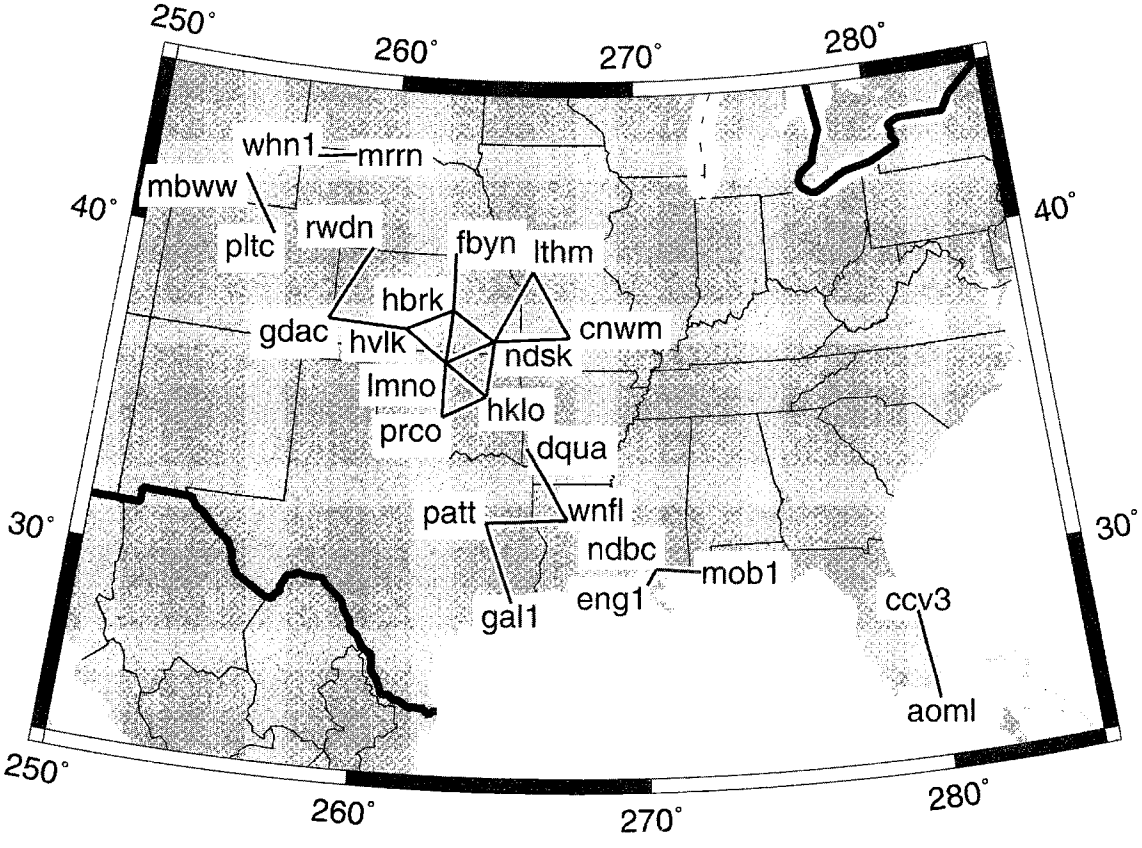

FIGURE 1. Baselines analyzed in this study.

TABLE 1

Observed baselines, baseline lengths, and uncertainty associated with free station heights

Baseline Number	Fixed Station	Free Station	Length (km)	Free Station Height Uncertainty 1.96 σ_{height} (cm)
1	eng1	ndbc	62	2.3
2	mrrn	whn1	135	1.4
3	mob1	ndbc	153	2.9
4	hklo	prco	170	1.8
5	hbrk	hvlk	175	1.6
6	hbrk	ndsk	178	1.8
7	hvlk	lmno	180	1.4
8	hbrk	lmno	180	1.9
9	lmno	ndsk	181	1.7
10	hklo	lmno	183	1.3
11	lmno	prco	189	1.4
12	hklo	ndsk	190	1.0
13	fbyn	hbrk	197	1.7
14	mbww	pltc	227	1.1
15	cnwm	ndsk	260	1.9
16	lthm	cnwm	261	1.7
17	gdac	hvlk	271	1.6
18	lthm	ndsk	275	1.4
19	patt	wnfl	278	3.3
20	dqua	wnfl	283	3.1
21	gal1	patt	287	2.1
22	gdac	rwdn	289	1.5
23	ccv3	aoml	304	3.0

and height (i.e., the standard pressure lapse rate), and the humidity at a constant 50%.

The scope of this study includes 23 baselines within the National CORS (Continuously Operating Reference Station) network that is managed by NOAA's National Geodetic Survey (NGS) (see Figure 1 and Table 1). High-precision continuously operating ground-based meteorological stations (termed "met stations" hereafter) are collocated with each of the GPS stations involved in these baselines. Given this GPS hardware and these sources of NAD, the basic strategy was to analyze the GPS data using each of three weather models to determine the effect of these different models on the precision of the estimated ellipsoidal heights.

COMPUTING THE NEUTRAL ATMOSPHERIC DELAY

Scientists have observed the neutral atmospheric delay with varying levels of certainty using a variety of techniques including radiosonde, water vapor radiometry, very long baseline interferometry, and GPS (Bevis et al., 1992). The GPS-based method relevant to this study relies on the basic assumption that the troposphere is azimuthally symmetric. Further, it assumes the NAD is composed of a hydrostatic (dry) component and a non-hydrostatic (wet) component.

The dry component is commonly determined from the measured weight of the atmosphere; and the wet component from the distribution of water vapor in the atmosphere and the atmospheric temperature. The NAD components are modeled by introducing two GPS signal delays that are oriented in the zenith direction.

The dry NAD component is modeled by the zenith dry delay, Z_D, and the wet component is modeled by the zenith wet delay, Z_W. Since GPS signals pass through more of the neutral atmosphere as satellite elevation angles decrease, mapping functions are commonly used to obtain the slant delay $T(\alpha)$ as a function of the satellite's elevation angle, α. That is,

$$T(\alpha) = m_D(\alpha) * Z_D + m_W(\alpha) * Z_W \qquad (1)$$

where m_D is the mapping function associated with the zenith dry delay and m_W is the mapping function associated with the zenith wet delay. The mapping function m_W is designed for lower levels of the troposphere where the bulk of the wet delay resides, whereas m_D is designed for levels extending from the antenna to the upper troposphere/lower stratosphere.

While several wet and dry delay models exist (Mendes, 1999), only models relevant to this study are presented here.

When using the Seasonal model, we are provided with values for surface pressure, surface temperature, and surface relative humidity. We then employ the time-honored Saastamoinen (1972) model to convert these values into Z_D and Z_W. When using the MAPS model, we are provided with the surface temperature and the quantity of precipitable water vapor (*PWV*) in a vertical column of air (expressed in units of length) at each node of a grid having a 40-km spacing. We interpolate these gridded values to obtain corresponding values at the points of interest. Moreover, we obtain the surface pressure at points of interest directly from a barometer. Again we use the Saastamoinen model to obtain Z_D. For obtaining Z_W, however, we convert surface temperature and PWV via the equation of Bevis et al. (1992):

$$Z_W = \Pi * PWV \tag{2}$$

where Π is roughly equal to 6.4. Π is a function of the mean atmospheric temperature, T_m, and several constants and is expressed as

$$\Pi = \frac{10^6}{\rho_o R_v (k_3 / T_m + k_2')} \tag{3}$$

where ρ_o is the density of water, R_v is the specific gas constant for water vapor, and k_2' and k_3 are refractivity constants. T_m exhibits seasonal and geographical variation that can be determined using simple linear regression of the form

$$T_m = Intercept + Slope * T_s \tag{4}$$

where T_s is surface temperature (Ross & Rosenfeld, 1997). Illustrations of the 11 radiosonde (weather balloon) launch sites and the corresponding annual long-term slopes and intercepts for the Ross and Rosenfeld (1997) data are provided in Figures 2 and 3, respectively. T_m was determined throughout this study by interpolation of Ross and Rosenfeld's (1997) monthly data.

When using the GPS-IPW model, we are provided with the zenith total delay, Z_T, which equals $Z_D + Z_W$. Again, we measure surface pressure directly and convert this pressure to Z_D via the Saastamoinen model. We then obtain Z_W via the equation $Z_W = Z_T - Z_D$.

DATA PROCESSING

We processed the GPS data and various sources of weather information with software developed at NGS entitled "Program for the Adjustment of GPS Ephemerides (PAGES)" (Mader et al., 1995). PAGES is a production and research tool employed for a variety of NGS products including high-precision GPS orbit determination and the determination of daily National CORS positions.

The basic observation used in this study is the ionosphere-free, double-difference phase observation (Seeber, 1993, p. 259). We processed the GPS data with a 30-s sampling rate and with a 15-degree cutoff angle, using precise GPS orbits disseminated by the IGS (Internation-

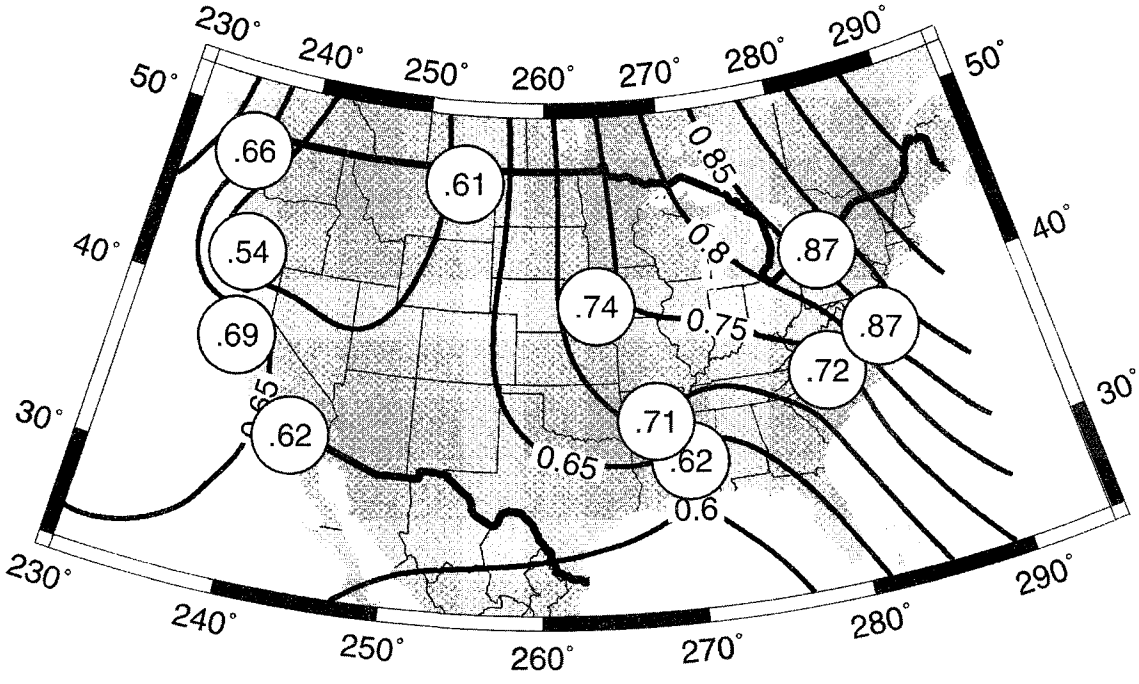

FIGURE 2. Annual long-term regression slopes from Ross and Rosenfeld (1997).

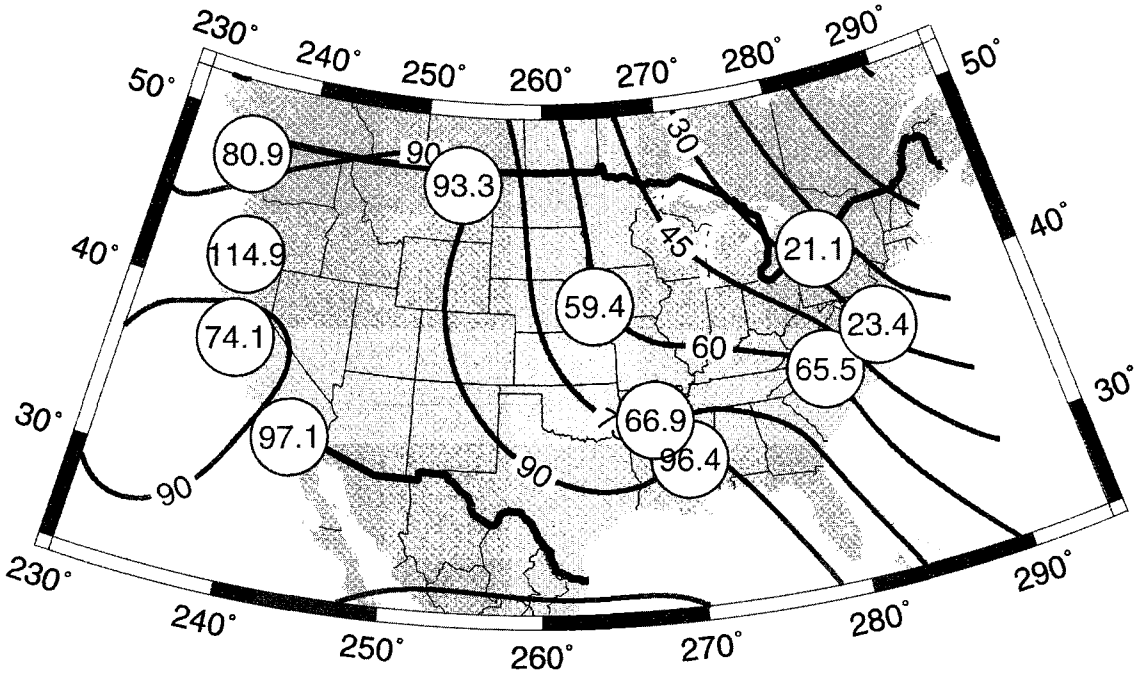

FIGURE 3. Annual long-term regression intercepts from Ross and Rosenfeld (1997).

al GPS Service). The Neill (1995) tropospheric mapping functions were employed. The Schwiderski ocean tide loading model was used to model systematic height variations caused by ocean tides, while solid-earth tidal displacements were modeled by a method described in Cartwright and Taylor (1971). Due to short session lengths and medium-length baselines, attempts to resolve ambiguities to integer values were not made and, consequently, "float" solutions were determined. Although PAGES permits multibaseline processing, each baseline in this study was processed as a single baseline.

PAGES offers various strategies for modeling NAD when processing GPS data. The fundamental input to each strategy consists of the wet, dry, and total delays that comprise three interdependent components of the NAD. Given this fundamental input, PAGES supports either (1) a "Fixed" solution where the NAD nuisance parameters are not estimated or (2) a solution where the NAD nuisance parameters are estimated. In the latter case, the NAD nuisance parameters may be completely unconstrained, or they may be constrained to within some uncertainty. Furthermore, nuisance parameter estimation may occur in either a relative or absolute sense. Relative parameter estimation implies NAD nuisance parameter estimation at one or more station(s) with the remaining station(s) held fixed, whereas absolute parameter estimation implies NAD nuisance parameter estimation at each station (Figure 4). Mikhail (1976) describes constrained and unconstrained parameter estimation.

Because the wet delay experiences rapid temporal and spatial variation relative to the dry delay, PAGES associates NAD nuisance parameter estimation with the wet delay. The NAD nuisance parameters lie within the double difference phase observation equation which is expressed as

$$\Phi_{ij}^{kl} = \rho_{ij}^{kl} + \lambda N_{ij}^{kl} - I_{ij}^{kl} + T_{ij}^{kl} + \varepsilon_{ij}^{kl} \qquad (5)$$

where

Φ_{ij}^{kl} = double difference phase observable in units of length
i,j = indices for the i-th and j-th receiver, respectively
k,l = indices for the k-th and l-th satellite, respectively
ρ_{ij}^{kl} = double difference range
λ = wavelength of the carrier phase
N_{ij}^{kl} = double difference ambiguity
I_{ij}^{kl} = double difference ionospheric delay
T_{ij}^{kl} = double difference neutral atmospheric delay, and
ε_{ij}^{kl} = error term.

The embedded NAD nuisance parameters associated with stations i and j (denoted as $\delta Z_{w,i}$ and $\delta Z_{w,j}$, respectively) appear in the one-way neutral atmospheric delays which comprise $T_{ij}^{kl} = [T(\alpha_i^k) - T(\alpha_i^l)] - [T(\alpha_j^k) - T(\alpha_j^l)]$. For example, one of the four delays, $T(\alpha_i^k)$, between station i and satellite k is expressed with the nuisance parameter for station i in linearized form as

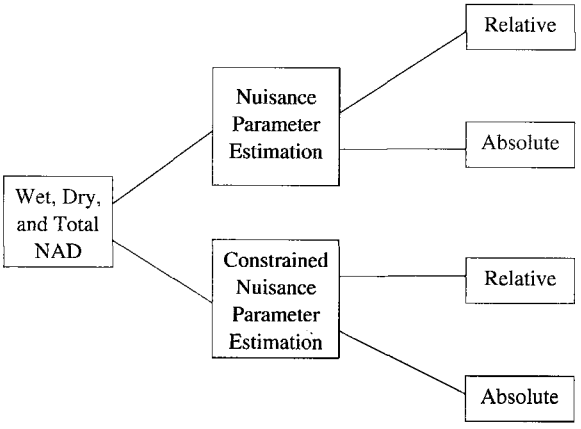

FIGURE 4. Various strategies for modeling the neutral atmospheric delay.

$$T(\alpha_i^k) = m_D(\alpha_i^k)Z_{D,i} + mw(\alpha_i^k)(Z_{W,i} + (\frac{\partial \Phi_{ij}^{kl}}{\partial Z_{W,i}})\delta Z_{W,i}) \quad (6)$$

A similar expression can be derived for $T(\alpha_i^l)$. The NAD nuisance parameter, $\delta Z_{W,j}$, for station j appears in the corresponding expressions for $T(\alpha_j^k)$ and $T(\alpha_j^l)$.

To better model the time-dependent nature of the NAD parameters, the relative and absolute parameter estimation strategies may be further defined in terms of the frequency of parameter estimation. One simple strategy used in this study was to ignore the time-varying nature of the NAD and simply estimate a single constant nuisance parameter at a given station for the entire observing session. A second model used in this study was the piecewise-linear (PWL) continuous model that is designed to honor the time-dependent behavior of the NAD by establishing two or more NAD parameter estimates at a given station for the entire observing session. Lancaster and Salkauskas (1986, p. 73) describe a piecewise-linear model.

DESCRIPTION OF EXPERIMENTS

The GPS observations used in this study were obtained for 23 baselines operating within the National CORS network over a 34-day period extending from 3 July to 6 August 1999 (day of year 184–218) (Figure 1). The analysis was performed on stations where both GPS and surface meteorological observations were available at each station. The typical met station observations include: (1) atmospheric pressure (σ = ±0.1 mb), (2) atmospheric temperature (σ = ±0.1° C), and (3) relative humidity (σ = ±1%) with 1-min sampling rate being common. The scope of the experiments included four session lengths and three primary input sources of NAD. The GPS data were obtained by extracting specific spans of data from 24-hr files available on the National CORS web server (http://www.ngs.noaa.gov/CORS/) in ½-hr, 1-hr, 2-hr, or 4-hr spans. The three sources of NAD are the Seasonal model, the MAPS model, and the GPS-IPW model. A summary of the three NAD sources appears in Table 2.

The three sources of NAD were analyzed with various strategies, ultimately leading to a grand total of 11 analysis methods (Table 3). Methods 1 through 3 represent traditional methods that have been routinely and successfully employed by NGS in the past, methods 4 through 10 are based on the MAPS model, and method 11 is based on the GPS-IPW model.

To evaluate the performance of the 11 methods, a "known" ellipsoidal height was computed for each of 23 free stations, one for each of the 23 baselines. This known height was defined by the sample mean of 34 highly precise 24-hr GPS baseline solutions. The ellipsoidal height standard deviations associated with the 23 free stations are presented in Table 1.

TABLE 2

Sources of neutral atmospheric delay in this study

Source of NAD	*Seasonal*		*MAPS & Barometer*		*GPS-IPW*	
Technique/ Equipment for Determining NAD	Historical Observations		Numerical Weather Model	Barometer	Post-Processed GPS Data	Barometer
Generated Meteorological Product	Surface Temp. & Humidity	Surface Pressure	Precipitable Water, Surface Temp.	Surface Pressure	n/a	Surface Pressure
NAD Products	Z_W	Z_D	Z_W	Z_D	Z_T	Z_D

TABLE 3

Neutral atmospheric delay parameterization

Analysis Method Number	Neutral Atmospheric Delay Model	Session Length (hr)	Number of Nuisance Parameters		Technique
			Fixed Station	Free Station	
1	Fixed Seasonal	½	0	0	N/a
		1	0	0	N/a
		2	0	0	N/a
		4	0	0	N/a
2	Relative Seasonal	½	0	1	Constant
		1	0	1	Constant
		2	0	2	2-hr PWL*
		4	0	3	2-hr PWL*
3	Absolute Seasonal	1/2	1	1	Constant
		1	1	1	Constant
		2	2	2	2-hr PWL*
		4	3	3	2-hr PWL*
4	Fixed MAPS & Barometer (M&B)	Same as Fixed Seasonal			
5,6,7	Relative M&B w/ 2-, 5-, and 10-cm constraints	Same as Relative Seasonal but NAD parameters constrained			
8,9,10	Absolute M&B w/ 2-, 5-, and 10 cm-constraints	Same as Absolute Seasonal but NAD parameters constrained			
11	Fixed GPS-IPW	Same as Fixed Seasonal			

*PWL = Piecewise Linear

ANALYSIS OF RESULTS

An initial examination of the ellipsoidal height results revealed several outliers caused by a number of factors such as multipath, insufficient observational data, rank deficiency, etc. Since outlying heights would corrupt our interpretation of the results, we eliminated outliers from further analysis when they deviated from the sample mean by more than 4 times the sample standard deviation (i.e., a 4σ criterion). We analyzed 44 groups of data and we generally found that 1–2% of the ellipsoidal heights exceeded the 4σ criterion (Table 4).

TABLE 4

Percentage of outliers exceeding 4σ criterion

	Session Length ½ hr (percent)	1 hr (percent)	2 hr (percent)	4 hr (percent)
Fixed Seasonal	1.0	0.5	0.6	0.4
Relative Seasonal	3.3	1.4	1.2	0.9
Absolute Seasonal	4.7	2.0	1.5	1.0
Fixed M&B	0.8	0.5	0.5	0.5
Relative M&B (2-cm Constraint)	1.0	0.5	1.2	1.2
Absolute M&B (2-cm Constraint)	1.1	0.6	1.2	1.2
Relative M&B (5-cm Constraint)	1.5	1.2	1.5	1.5
Absolute M&B (5-cm Constraint)	1.4	1.2	1.3	1.4
Relative M&B (10-cm Constraint)	1.8	1.3	1.3	1.6
Absolute M&B (10-cm Constraint)	2.1	1.3	1.4	1.4
Fixed GPS-IPW	2.1	2.0	2.1	2.3

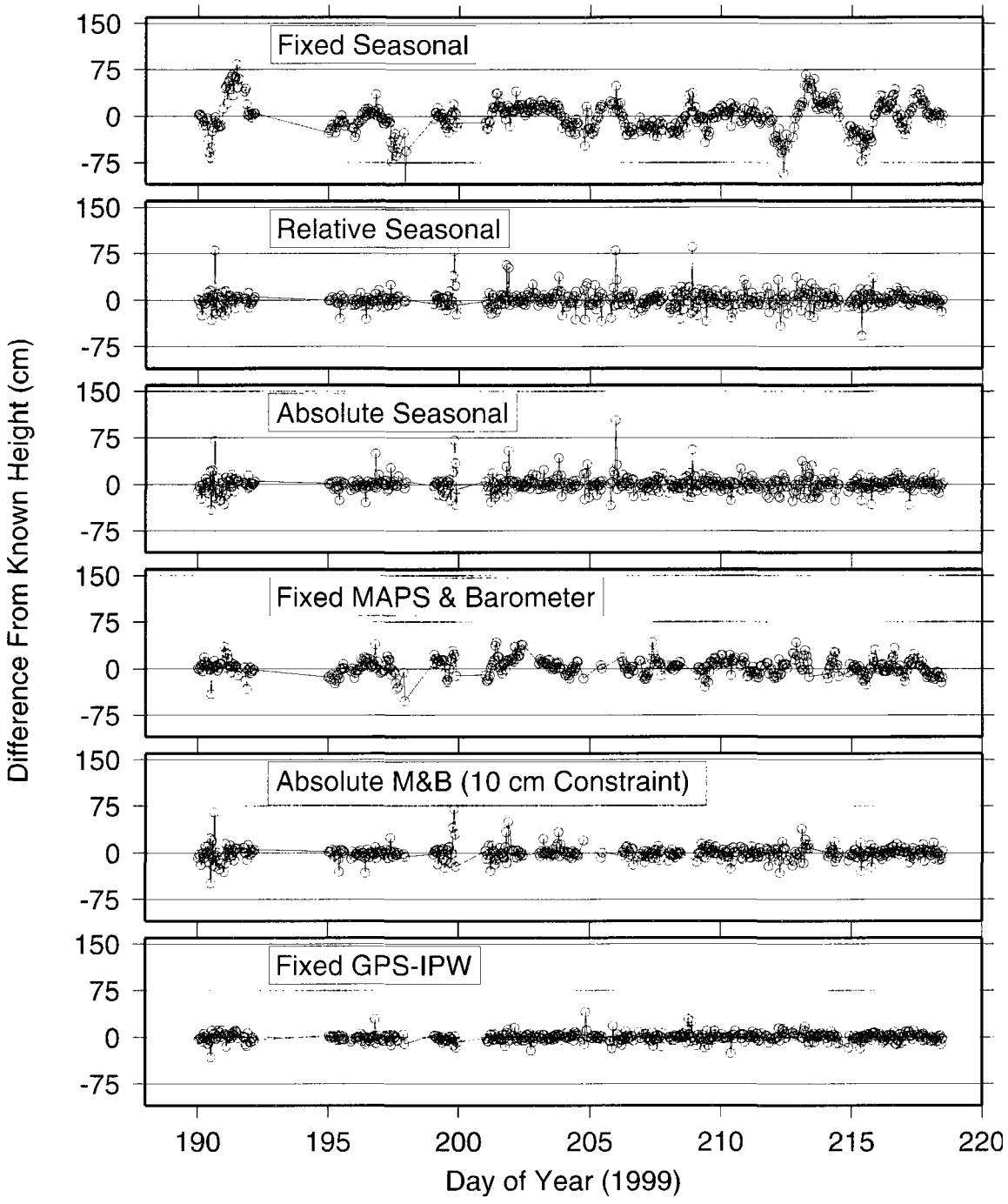

FIGURE 5. Time-series plots for lthm-cnwm, 261-km, 1-hr session length.

We examined the experimental results using four different techniques, each yielding unique insight into behavior of the various weather models. The first technique is demonstrated through 1-hr time-series plots of station heights for a single 261-km baseline (Lathrop, Missouri [lthm] to Conway, Missouri [cnwm]) using six of the analysis methods (Figure 5). Methods 5–9 are not presented due to their similarity with method 10, the Absolute Maps and Barometer (M&B) model with 10-cm constraints. The time-series plots in Figure 5 reveal that station height estimation is considerably affected by the method of modeling the NAD. For this example baseline, the Fixed Seasonal model height differences reflect unmodeled systematic changes in the NAD, suggesting that the Fixed Seasonal model inadequately characterizes temporal variation in the weather; or equivalently, the temporal variation in NAD.

By contrast, height differences associated with the Relative Seasonal and Absolute Seasonal models indicate that

temporal variation in NAD is adequately accommodated by estimating values for the NAD nuisance parameters. The Fixed M&B method appears to address large temporal variations in the NAD better than the Fixed Seasonal method; however, substantial height variation still exists for the Fixed M&B method due to imprecise modeling of the NAD.

Finally, the Fixed GPS-IPW method shows little height variation and little bias from the adopted height. The Fixed GPS-IPW heights are difficult to assess, however, due to the incestuous nature by which they were computed. In particular, the GPS-IPW neutral atmospheric delays are generated using the same GPS observations and the same GPS hardware (i.e., antennas and receivers) that are used by PAGES to compute ellipsoidal heights. Consequently, we suspect that unmodeled systematic errors (such as multipath, antenna phase center variation, and higher-order ionospheric effects, for example), which are common to both the GPS-IPW processing and the PAGES processing, are improperly represented in our analysis of the Fixed GPS-IPW heights. Given this incestuous analysis, we believe the precision of the Fixed GPS-IPW heights is optimistic. In contrast to the GPS-IPW model, the MAPS and Seasonal models are developed independently of GPS observations and hardware.

The second technique attempts to identify trends that may be baseline-length dependent. Figure 6 illustrates the

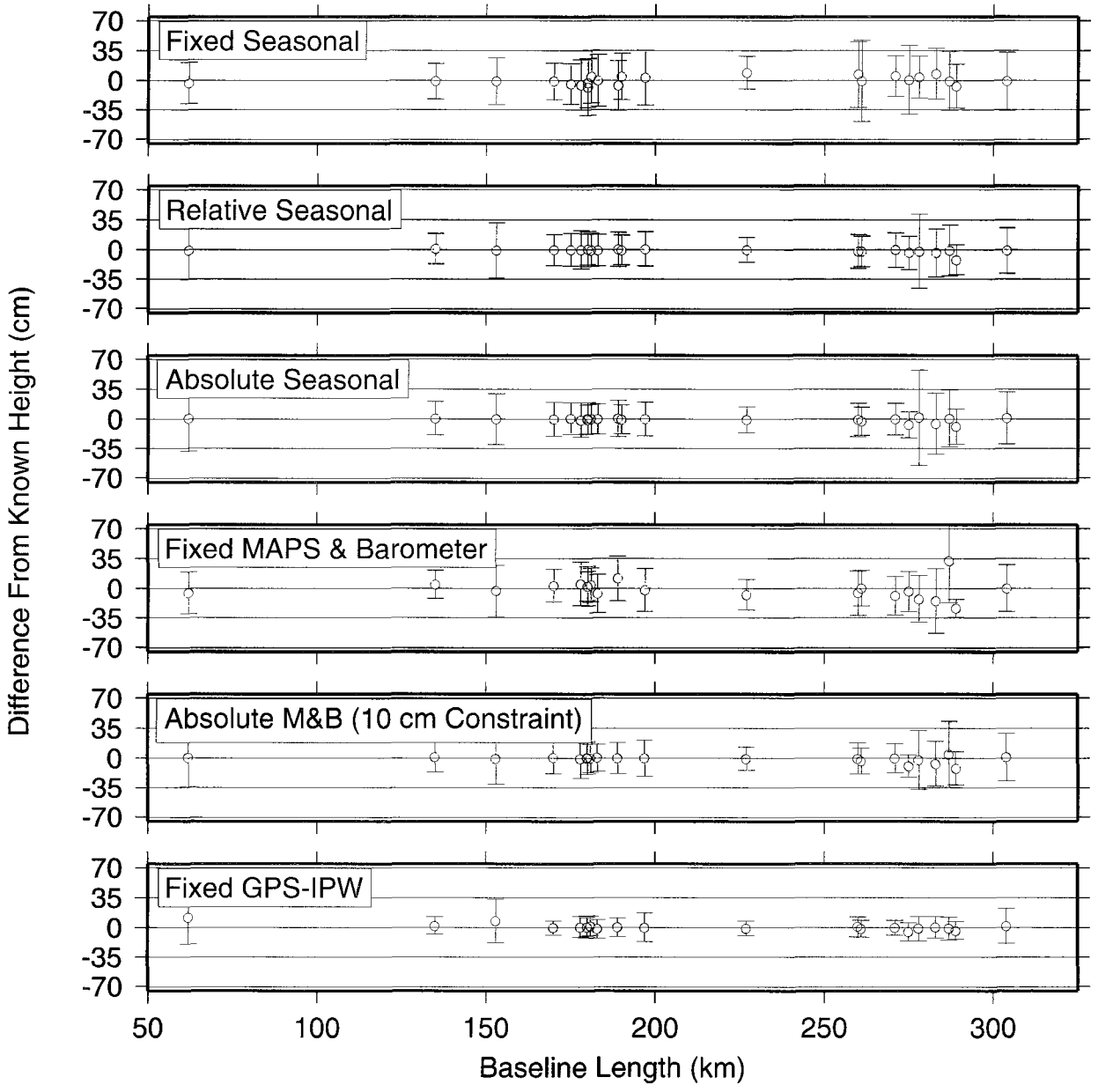

FIGURE 6. Height difference versus baseline length, 1-hr sessions, 1σ error bars.

mean height differences for the 23 baselines and for six analysis methods evaluated at 1-hr session lengths. Like the time-series plots in Figure 5, the Fixed Seasonal model heights differ from the adopted height, indicating poor NAD modeling for many baselines. Given the caveats related to the GPS-IPW model mentioned earlier, the Fixed GPS-IPW model precisely models the NAD and consequently exhibits little variation and little bias from the adopted height. The magnitudes of the error bars in Figure 6 appear to increase mildly as baseline length increases.

The third and fourth techniques provide an overall perspective of the experimental results by illustrating height variation as a function of session length (Figures 7 and 8, respectively). We generated these two figures by averaging results for the 23 baselines. The relative quality of the three models (Seasonal, M&B, and GPS-IPW) is best revealed by examining height precision when no NAD nuisance parameters are estimated. For each of the four session lengths considered here, the Fixed M&B method (curve marked with solid rectangles in Figure 7) yields a height precision that is approximately 6 cm better than the height precision obtained using the Fixed Seasonal method (curve marked by solid triangles). Finally, for each session length, the Fixed GPS-IPW method (curve marked by solid circles) yields a height precision that is approximately 18 cm better than the height precision obtained using the Fixed Seasonal method. As previously mentioned, however, the GPS-IPW model was derived using the same GPS data that we processed to obtain our heights.

The three weather models yield similar height precision when long session lengths are coupled with nui-

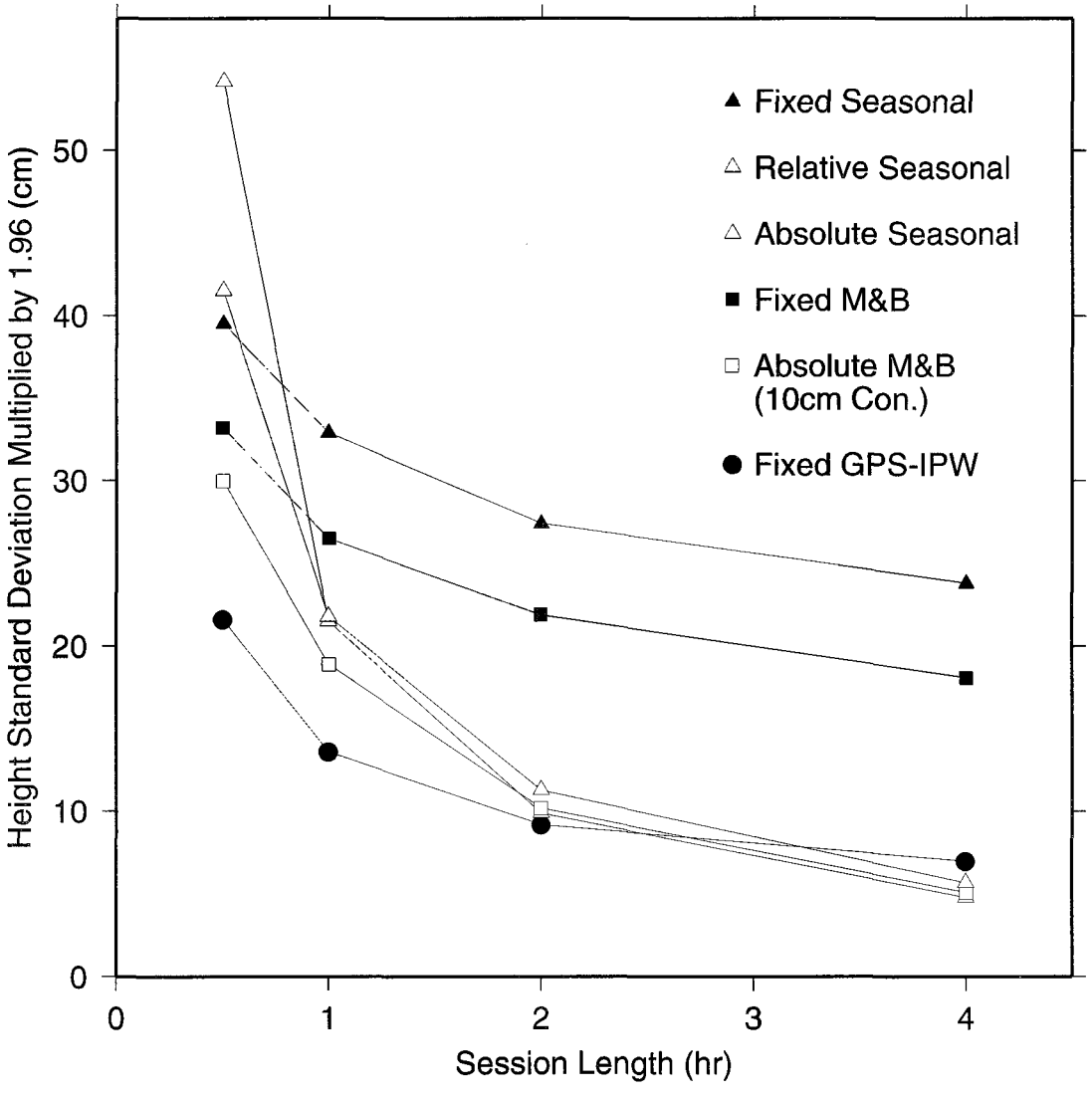

FIGURE 7. Height standard deviation versus session length.

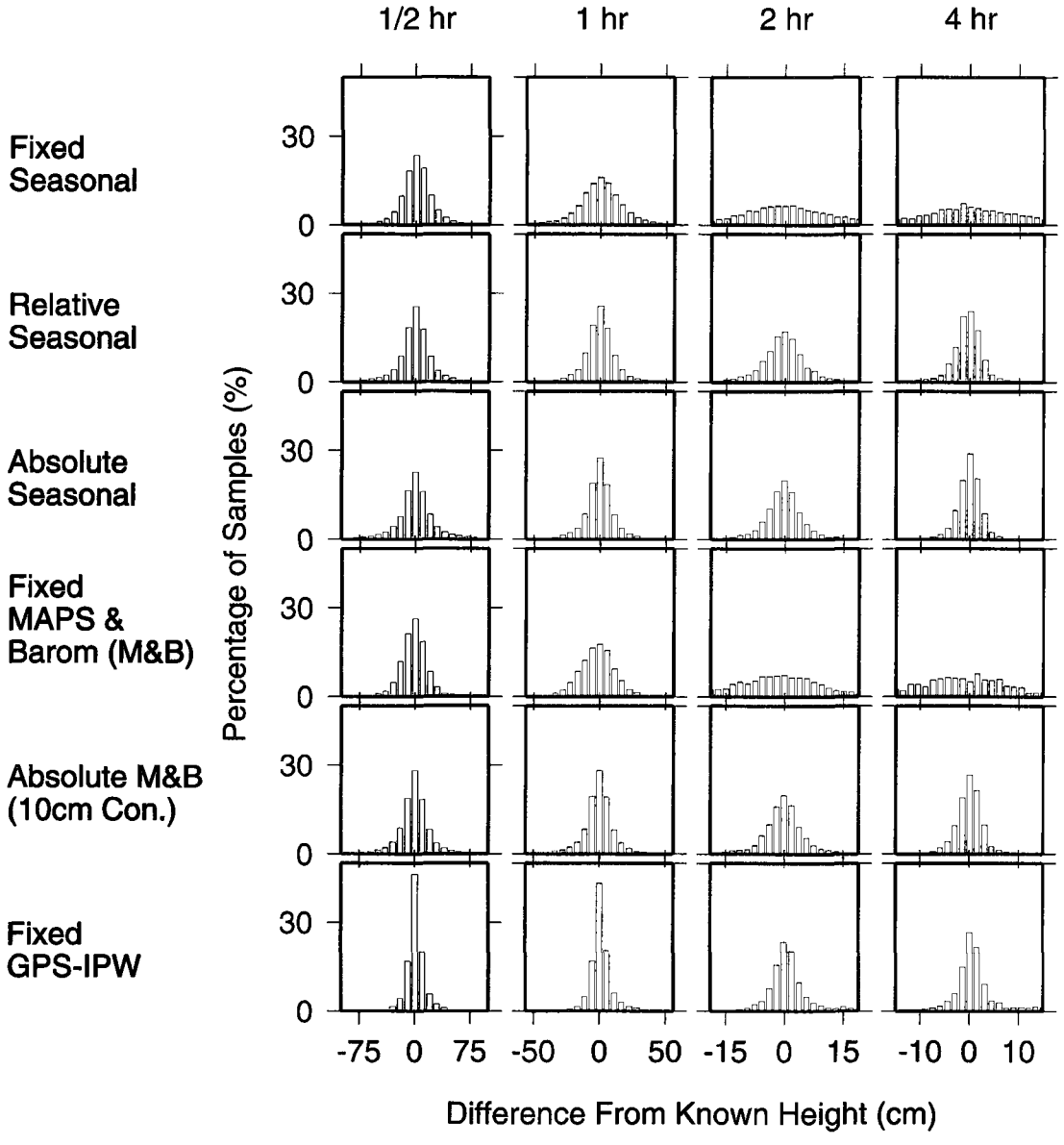

FIGURE 8. Height difference histograms for six analysis methods and all session lengths.

sance parameter estimation. Indeed, Figure 7 displays how the Absolute Seasonal method (curve marked by open triangles) does just as well as the Absolute M&B method (curve marked by open rectangles) for the 2- and 4-hr session lengths. Session lengths shorter than two hours contain insufficient GPS data to estimate both heights and nuisance parameters, and hence more accurate weather information is needed to obtain more precise heights for these shorter session lengths.

Note that although the inclusion of nuisance parameters is beneficial for longer session lengths, the inclusion of these parameters may be detrimental for extremely short session lengths. In particular, the Absolute Seasonal method (open triangles) performs worse than the Fixed Seasonal method when the session length is only ½-hr long. The Relative Seasonal method (shaded triangles) yields a height precision intermediary to the Fixed Seasonal method and the Absolute Seasonal method for ½-hr session lengths because the Relative Seasonal method involves fewer nuisance parameters than the Absolute Seasonal method.

The fourth technique employs height difference histograms to illustrate the relative performance of the six methods. The histograms reveal similarities in structure between the Seasonal and M&B models, indicating that the two models perform at similar levels of precision. Common statistical measures associated with these histograms, such as the sample mean, are presented in Table

TABLE 5

Overall statistical measures from experiments

	Session Length															
	½ hr				1 hr				2 hr				4 hr			
	n	$\bar{x}$ (cm)	1.96 $\sigma_{\bar{x}}$ (cm)	1.96 σ_x (cm)	n	$\bar{x}$ (cm)	1.96 $\sigma_{\bar{x}}$ (cm)	1.96 σ_x (cm)	n	$\bar{x}$ (cm)	1.96 $\sigma_{\bar{x}}$ (cm)	1.96 σ_x (cm)	n	$\bar{x}$ (cm)	1.96 $\sigma_{\bar{x}}$ (cm)	1.96 σ_x (cm)
Fixed Seasonal	19157	0.7	0.3	39.5	9384	0.6	0.3	32.9	4489	0.5	0.4	27.1	1979	0.6	0.5	23.8
Relative Seasonal	18707	0.4	0.3	41.5	9303	0.8	0.2	21.8	4460	0.8	0.2	11.3	1969	0.8	0.1	5.7
Absolute Seasonal	18432	0.1	0.4	54.2	9245	-0.4	0.2	21.5	4448	-0.2	0.1	9.9	1966	-0.1	0.1	4.8
Fixed M&B	12729	-2.2	0.3	33.2	6300	-2.1	0.3	26.5	3057	-1.8	0.4	21.9	1357	-1.4	0.5	18.1
Relative M&B (2-cm Constraint)	12708	-2.0	0.3	31.1	6286	-1.5	0.3	20.8	3012	0.0	0.2	10.6	1332	0.0	0.1	5.4
Absolute M&B (2-cm Constraint)	12928	-1.8	0.3	30.0	6290	-1.2	0.2	18.9	3021	-0.1	0.2	10.2	1340	-0.1	0.1	5.1
Relative M&B (5-cm Constraint)	12859	-0.9	0.2	27.8	6243	-0.4	0.2	18.8	2942	0.0	0.2	10.4	1193	0.0	0.2	5.3
Absolute M&B (5-cm Constraint)	12881	-0.8	0.3	29.5	6249	-0.4	0.2	19.2	3016	-0.1	0.2	10.1	1337	-0.1	0.1	5.0
Relative M&B (10-cm Constraint)	12832	-0.4	0.3	37.2	6233	-0.3	0.3	20.9	2945	0.0	0.2	10.6	1195	0.0	0.2	5.3
Absolute M&B (10-cm Constraint)	12791	-0.5	0.3	37.5	6246	-0.3	0.3	20.9	3016	-0.2	0.2	10.1	1340	-0.1	0.1	5.0
Fixed GPS-IPW	12714	1.2	0.2	21.6	5975	0.8	0.2	13.6	2667	0.8	0.2	9.2	1023	0.7	0.2	7.0

5 where n denotes the number of samples for each method, $\bar{x}$ denotes the sample mean, σ_x denotes the sample standard deviation, and $\sigma_{\bar{x}}$ denotes the standard deviation of the mean. The number of available samples for each of the analysis methods vary due to interruptions/outages in the available data and due to outliers in the ellipsoidal heights mentioned earlier.

DISCUSSION

The MAPS weather model appears to supply GPS users with valuable information concerning the behavior of the wet NAD. However, since two components of the NAD are necessary to completely characterize the NAD in the simplified models presented in this paper, GPS users will desire a complete description of the NAD and will therefore desire additional information concerning either the dry NAD or the total NAD. To this end, future efforts are needed to precisely determine the dry or total NAD without the requirement for additional hardware (i.e., a barometer) in the field. NGS personnel are currently investigating alternative means of supplying GPS users with precise NAD estimates for locations within the contiguous United States. To that end, NGS is investigating the ever growing National CORS network as a potential source of precise total NAD values.

CONCLUSIONS

The primary conclusion of this study is that the a priori MAPS weather data, coupled with high-precision atmospheric pressure observations, supplies valuable information to GPS users that can lead to improved height precision under certain conditions. These conditions include baselines ranging in length from 62 to 304 km and for session lengths 2 hours and less. Unfortunately, GPS users must obtain precise atmospheric pressure observations to model the zenith dry delay in order to obtain improved height precision with MAPS. The reason for this inconvenience is that MAPS only provides reliable estimates of the quantities that lead to zenith wet delay in its current status.

The required precision of atmospheric pressure observations depends on the application; however, a general rule of thumb is that a 0.5-mb error in atmospheric pressure roughly leads to a 1.2-mm error in zenith dry delay at sea level (Brunner & Welsh, 1993). For session lengths greater than 2 hours, we conclude that sufficiently precise NAD modeling for geodetic activities may be achieved by coupling nuisance parameter estimation with the relatively crude Seasonal model.

ACKNOWLEDGMENTS

The first author wishes to acknowledge support from the NOAA Research Participation Program at the National Geodetic Survey, which is administered by the Oak Ridge Institute for Science and Education. Also, the authors wish to thank Mike Cline, Steve Hilla, Dennis Milbert, and Charles Schwarz for their comments on an earlier version of this paper. Several figures were created using the Generic Mapping Tools (Wessel & Smith, 1991).

REFERENCES

Bevis, M., Businger, S., Herring, T., Rocken, C., Anthes, R., & Ware, R. (1992). GPS meteorology: remote sensing of the atmospheric water vapor using the global positioning system. J. Geophys. Res., 97 (D14), 75–94.

Brunner, F., & Welsh, W. (1993). Effect of the troposphere on GPS measurements. GPS World, 4 (1), 42–51.

Cartwright, D.E., & Edden, A.C. (1973). Corrected tables of tidal harmonics, Geophys J.R. Astr. Soc., 33, 253–264.

Cartwright, D.E., & Taylor, R.J. (1971). New computations of the tide-generating potential. Geophys. J.R. Astr. Soc., 23, 45–74.

Fullerton, N. (Ed.). (1999). FSL in review. NOAA Environmental Research Laboratories, Boulder, CO.

Herring, T. (1995). Personal communication. FORTRAN code developed at MIT by T. Herring and later modified and adapted by J. Ray at the National Geodetic Survey in 1995.

Lancaster, P., & Salkauskas, K. (1986). Curve and surface fitting: an introduction. New York: Academic Press, Harcourt Brace Jovanovich.

Mader, G.L., Schenewerk, M.S., Ray, J.R., Kass, W.G., Spofford, P.R., Dulaney, R.L., & Pursell, D.G. (1995). GPS orbit and earth orientation parameter production at NOAA for the International GPS Service for Geodynamics for 1994. In J.F. Zumberge et al. (Eds.), International GPS Service for Geodynamics 1994 Annual Report (pp. 197–212). Jet Propulsion Lab., California Institute of Technology, Pasadena, CA.

Mendes, V. (1999). Modeling the neutral-atmospheric propagation delay in radiometric space techniques. Ph.D. dissertation, Department of Geodesy and Geomatics Engineering Technical Report No. 199, University of New Brunswick, Fredericton, New Brunswick, Canada.

Mikhail, E. (1976). Observations and least squares. Lanham, MD: University Press of America, Harper & Row.

Niell, A.E. (1995). Global mapping functions for the atmosphere delay at radio wavelengths, J. Geophys. Res., 101 (B2), 3227–3246.

Ross, R., & Rosenfeld, S. (1997). Estimating mean weighted temperature of the atmosphere for Global Positioning System applications. J. Geophys. Res., 102 (21), 719–721, 730.

Saastamoinen, J. (1972). Atmospheric correction for the troposphere and stratosphere in radio ranging of satellites. In S.W. Henriksen et al. (Eds.), The use of artificial satellites for geodesy, Geophys. Monogr. Ser. 15 (pp. 247–251). Washington, DC: American Geophysical Union.

Seeber, G. (1993). Satellite geodesy: foundations, methods, and applications. de Gruyter.

Wessel, P., & Smith, W.H.F. (1991). Free software helps map and display data. EOS Trans. Amer. Geophys. U., 72, 441, 445–446.

BIOGRAPHIES

John Marshall is a geodesist at the National Geodetic Survey. He has interests in atmospheric modeling and ambiguity resolution for medium-scaled networks. He received a Ph.D. in surveying engineering at Purdue University in 1998.

Dr. Mark Schenewerk received his Ph.D. in astronomy from the University of Illinois in 1986. From 1986 through 1987 he worked as a system scientist for the National Radio Astronomy Observatories supporting geodetic measurements with VLBI while continuing his research in radio astronomy. In 1987, Dr. Schenewerk joined NOAA/National Geodetic Survey where he provides technical support for and conducts research on GPS ephemeris generation.

Richard A. Snay is Program Manager of the National CORS system. He received his Ph.D. in mathematics from Indiana University in 1972 and has served as a geodesist with the National Geodetic Survey since 1974. He also models crustal motion to support accurate time-dependent positioning.

Seth Gutman is Chief, GPS-Met Observing Systems Branch of the NOAA Forecast Systems Laboratory Demonstration Division. He is responsible for the development and testing of ground-based GPS meteorological observing systems, and facilitating their assessment as a possible next-generation upper-air observing system for NOAA. His graduate and undergraduate education was in solid earth geophysics at the University of California at Riverside and the University of Arizona at Tucson.

Peer Review: This paper has been peer-reviewed and accepted for publication according to the guidelines provided in the Information for Contributors.